TWMS J. App. and Eng. Math. V.16, N.7, 2026, pp. 901-918

MODELING EPIDEMIC SPREAD USING TIME-DEPENDENT GRAPH DIFFUSION EQUATIONS ON COMPLEX NETWORKS

G. SARMITHA[1], S. VIDYANANDINI[1*], M. B. SANJAY[2], ANUSHREE SHRIVASTAVA[3], RAVINDER SINGH KUNTAL[4], §

Abstract. Epidemic spread in real populations is shaped by changing contact patterns, uneven connectivity, and localized transmission, so static and uniformly mixed models are often not sufficient. Complex networks provide a stronger mathematical basis for representing these evolving interactions because they capture both structural heterogeneity and temporal variation. Existing research has examined temporal networks, multilayer epidemic systems, and graph-based transmission models, but many formulations still do not fully unify node-wise epidemic states, weighted graph diffusion, and time-dependent transmission in one solvable framework. A clear gap therefore remains in developing a mathematically consistent model that can represent epidemic propagation on evolving complex networks with both analytical and numerical clarity. This study addresses that gap by proposing a time-dependent graph diffusion model for epidemic spread. The paper focuses on developing the graph-mathematical formulation, deriving the governing equations, implementing an explicit numerical solution method, and testing the model on various network types, diffusion strengths, temporal transmission patterns, and intervention scenarios. Results demonstrate the significant impact of structure and time on epidemic spread, showing faster initial spread in scale-free networks, shifts in peak timing in evolving-contact graphs, and reduced outbreak severity under early intervention. The proposed framework offers a solid and practical basis for predicting epidemics on changing networks.

Keywords: epidemic modeling, graph diffusion, complex networks, temporal transmission, numerical simulation.

AMS Subject Classification: 05C82

[1] Department of Mathematics, College of Engineering and Technology, SRM Institute of Science and Technology, Kattankular, India.
[2] Department of Mathematics, SARBTM Government College Koyilandy, Kozhikode, Kerala, India.
[3] Kalinga University, Naya Raipur, Chhattisgarh, India.
[4] Department of Mathematics, Nitte (Deemed to be University), Nitte Meenakshi Institute of Technology (NMIT), Bengaluru, Karnataka, India.
e-mail: sg7675@srmist.edu.in, ORCID: 0009-0004-3362-2751.
e-mail: vidyanas@srmist.edu.in, ORCID: 0000-0002-4812-3259.
e-mail: sanjaymb3@gmail.com; ORCID: https://orcid.org/0009-0009-1035-3268.
e-mail: ku.AnushreeShrivastava@kalingauniversity.ac.in, ORCID: 0009-0004-1474-5190.
e-mail: ravindercertain@gmail.com, ORCID: 0000-0003-1225-8108.
* Corresponding author.
§ Manuscript received: April 24, 2025; accepted: September 17, 2025.
TWMS Journal of Applied and Engineering Mathematics, Vol.16, No.7;

1. Introduction

Epidemic spread is a network-driven dynamical process because infection moves through nonuniform contact pathways rather than through a perfectly mixed population. Human interactions are shaped by transport systems, workplaces, schools, households, and community clusters, so the transmission structure is more naturally represented as a complex graph than as a single homogeneous compartment [1, 2]. In this study, the contact system is represented by a graph $G = (V, E)$, where V denotes the set of nodes and E denotes the set of epidemiologically relevant links. The weighted adjacency matrix is written as

$$A(t) = [a_{ij}(t)]_{N\times N}\,, \tag{1}$$

where $a_{ij}(t) \geq 0$ gives the time-dependent interaction strength between nodes i and j. The corresponding graph Laplacian is defined by

$$L(t) = D(t) - A(t), \tag{2}$$

where $D(t)$ is the diagonal degree matrix. This graph representation provides a mathematical basis for describing how infection pathways depend on connectivity and temporal change.

Temporal connectivity and community organization strongly influence epidemic timing and outbreak size, and these effects become more visible when the network changes during transmission [3]. Contact heterogeneity also changes the role of individual nodes because highly connected regions do not contribute to spread in the same way as weakly connected regions [4, 5]. Local interactions among adaptive agents can generate emergent system-level behavior even without central control [6]. These observations show that epidemic evolution should be studied as a coupled system of node states and network structure rather than as a purely averaged population process. A model that keeps both topology and time variation inside the governing equations is therefore more suitable for realistic epidemic analysis.

Many existing epidemic models still rely on static networks, coarse compartment averages, or simplified temporal updates, even though outbreak dynamics are sensitive to evolving link structure [1]. In several formulations, network connectivity is introduced only as a descriptive layer, while the main equations do not fully integrate time-varying diffusion over the graph with local epidemic reactions [7, 8]. Other models include temporal parameters but do not preserve a strong node-wise description of infection transfer across heterogeneous contact pathways. Such limitations make it difficult to capture delayed spread into peripheral communities, topology-driven threshold changes, and the redistribution of infectious pressure caused by changing interactions. A more unified operator-based formulation is therefore needed.

The central problem selected in this article is the modeling of epidemic propagation through a time-dependent graph diffusion system defined at node level. Instead of representing infection by a single global infected fraction, the model assigns a local epidemiological state to every node, which is written as

$$x_i(t) = \begin{bmatrix} S_i(t) \\ I_i(t) \\ R_i(t) \end{bmatrix}, \tag{3}$$

where $S_i(t)$, $I_i(t)$, and $R_i(t)$ denote the susceptible, infected, and recovered fractions at node i. The node-wise conservation condition is expressed as

$$S_i(t) + I_i(t) + R_i(t) = 1, \quad i = 1, 2, \ldots, N. \tag{4}$$

This choice narrows the study to a precise mathematical question: how node-level epidemic states evolve when both connectivity and transmission intensity vary with time.

This problem matters because real outbreaks are rarely uniform across a network. Hub-like nodes can trigger rapid transmission cascades, whereas weakly connected nodes may remain uninfected until much later, and adaptive behavior or mobility restrictions can change these pathways during the outbreak itself [9]. Forecasts that ignore such features can misestimate peak infection, outbreak duration, or the communities most exposed to secondary spread [2]. Real-time changes in distributed population states and movement patterns can also alter local demand and system response as conditions evolve [10]. A framework that accounts for time-dependent topology is therefore important not only for theoretical understanding but also for practical interpretation of intervention timing and network vulnerability. The need for this type of model becomes stronger when the contact system is heterogeneous and evolves during disease transmission.

The mathematical direction adopted here is to treat epidemic spread as a diffusion-reaction process on a time-dependent graph. In this view, graph diffusion captures the movement of infectious influence across links, while local reaction terms represent infection generation and recovery at each node, which is consistent with graph-based epidemic dynamics developed for temporal and multilayer systems [7, 9]. Graph-based learning studies have likewise shown that local structural relationships can strongly influence system-level outcomes [11]. The infected component at node i is described by

$$\frac{dI_i}{dt} = -\mu_i(t)I_i(t) + \kappa \sum_{j=1}^{N} a_{ij}(t)(I_j(t) - I_i(t)) + \beta_i(t)S_i(t)I_i(t), \tag{5}$$

where $\mu_i(t)$ is the recovery coefficient, $\beta_i(t)$ is the transmission coefficient, and κ is the graph diffusion strength. In vector form, the same structure becomes

$$\frac{d\mathbf{I}}{dt} = -\mu(t) \odot \mathbf{I}(t) - \kappa L(t)\mathbf{I}(t) + \beta(t) \odot \mathbf{S}(t) \odot \mathbf{I}(t), \tag{6}$$

where $\odot$ denotes element-wise multiplication. This formulation directly links epidemic growth to graph structure and time-varying node interactions.

Time dependence is included explicitly because both the edge structure and the effective transmission field can vary during an epidemic. Contact intensity may change because of behavior adaptation, intervention policies, seasonal effects, or mobility fluctuations, and these variations can alter epidemic thresholds and spreading routes on temporal networks [3]. To represent this mechanism, the incoming transmission field at node i is written as

$$\mathcal{T}_i(t) = \beta_i(t) \sum_{j=1}^{N} a_{ij}(t)I_j(t), \tag{7}$$

which combines local transmissibility with the infected influence arriving through the current network state. This expression makes the model sensitive to both neighbor infection levels and instantaneous edge strength. As a result, the formulation can describe outbreaks that evolve with the contact network instead of assuming a fixed transmission environment.

The proposed framework is intended to provide a mathematically consistent basis for simulation and analysis rather than only a descriptive network model. The combination of node-wise conservation, graph Laplacian diffusion, and temporal transmission variation creates a unified structure that can be used to study outbreak growth, network sensitivity, and topology-dependent epidemic behavior. This design also creates a direct path toward numerical solution procedures, parameter sweeps, and comparative tests across different

network classes. The model is therefore positioned as a bridge between classical epidemic equations and operator-based graph dynamics.

The main contribution of this work is the formulation of epidemic spread on complex networks through a time-dependent graph diffusion equation that preserves node-level epidemic balance while embedding transmission in an evolving graph operator. A second contribution is the integration of heterogeneous topology, temporal link variation, and local epidemic reactions within one compact mathematical framework. A third contribution is the creation of a structure that supports numerical investigation of dynamic outbreaks across multiple network scenarios and control settings. The next section develops the full methodology, including the governing equations, computational workflow, and simulation setup used in the study.

2. Methodology

The methodological framework is designed to translate the proposed epidemic concept into a mathematically complete and computationally solvable model. It establishes how the complex contact network is constructed, how node-level epidemic states are defined, how time-dependent graph diffusion equations are derived, and how these equations are solved numerically over successive time intervals. Methodologically, the framework defines the parameters, setting, and computational order necessary to propagate simulated epidemics on a network that is heterogeneous and evolving over time. The framework integrates the theory of graphs, the theory of dynamical systems, and numerical analysis into a coherent whole, allowing for both theoretical and simulation-based analysis.

2.1. **Network topology and epidemic state definition.**

A complex contact network provides the structural base of the proposed epidemic model because transmission does not occur in an empty space but through links connecting interacting nodes. In this work, each node represents an individual, group, or spatial unit, while each edge represents a possible transmission pathway whose strength may vary from one connection to another. This type of representation is suitable for epidemic systems where contact patterns are layered, location-dependent, and structurally heterogeneous [12]. The full network is written as $G = (V, E, W)$, where V is the node set, E is the edge set, and W represents the edge-weight structure. This representation is useful because it allows the model to distinguish between weak and strong contacts instead of treating all interactions as identical.

The contact relations inside the network are described by a weighted adjacency matrix so that the connectivity pattern can be handled in a clear mathematical form. If the network contains N nodes, the adjacency structure is written as

$$A = [a_{ij}]_{N\times N}\,, \tag{8}$$

where $a_{ij} \geq 0$ denotes the weight of the connection from node j to node i. A zero entry means that no direct epidemiological interaction exists between the two nodes, while a larger value indicates stronger contact intensity. This weighted form is important because epidemic spread on realistic networks depends not only on whether two nodes are connected, but also on how strongly they interact. A weighted adjacency representation is also consistent with higher-order spatial epidemic networks in which link intensity influences spreading behavior [13].

The degree structure of the graph is then obtained from the adjacency matrix so that the total influence acting on each node can be measured. For weighted networks, the degree of node i is defined by the sum of all edge weights connected to that node, and this

quantity is stored in the diagonal degree matrix

$$D = \mathrm{diag}(d_1, d_2, \ldots, d_N), \quad d_i = \sum_{j=1}^{N} a_{ij}. \tag{9}$$

The degree matrix plays an important role because it gives the total local connectivity surrounding each node. Nodes with large weighted degree are more exposed to incoming and outgoing infection influence than sparsely connected nodes. This difference later affects how infection pressure is redistributed through the network.

The graph Laplacian is introduced next because it is the main operator used to express diffusion-like movement across the network. It is defined as

$$L = D - A. \tag{10}$$

This operator compares the local degree effect with the direct connection pattern and therefore measures how a node differs from its neighborhood. In graph-based epidemic modeling, the Laplacian is especially useful because it converts the network into an operator form that can drive spread from one region of the graph to another. This operator-based view is especially relevant in structured network settings where spatial and topological effects influence epidemic flow.

Node-wise epidemic information is assigned by attaching a local state vector to each node rather than using only one global population average. For node i, the epidemiological state is written as

$$x_i(t) = \begin{bmatrix} S_i(t) \\ I_i(t) \\ R_i(t) \end{bmatrix}, \tag{11}$$

where $S_i(t)$, $I_i(t)$, and $R_i(t)$ represent the susceptible, infected, and recovered fractions at time t. This node-level structure is important because different parts of a heterogeneous network may experience different epidemic conditions at the same instant. A densely connected node may already have a high infected fraction while a weakly linked node may remain mostly susceptible. The local state formulation therefore preserves spatial and topological variation inside the model. The initialization of these node states is illustrated in Figure 1, where the complex network representation is shown together with the initial assignment of susceptible, infected, and recovered values over the nodes. The figure is

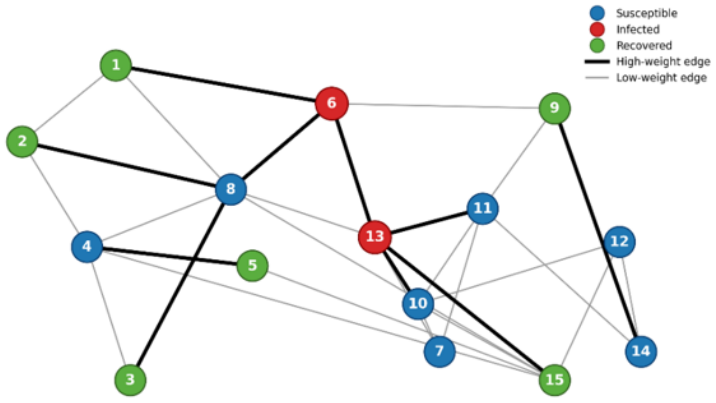

Figure 1. Complex network representation and node-wise epidemic state initialization

important because it visually links the graph structure to the epidemic state variables and shows how infection seeds are positioned before the time evolution begins. Node-wise initialization over a structured contact network is especially important when the starting outbreak is localized rather than uniformly distributed [12]. In this way, Figure 1 does not serve as a decorative diagram but as a direct visual counterpart to the adjacency, degree, Laplacian, and node-state definitions introduced in this subsection.

The definitions established above are sufficient to create the structural layer of the proposed model before any time-dependent epidemic dynamics are introduced. The graph G, adjacency matrix A, degree matrix D, Laplacian L, and node state vector $x_i(t)$ together form a complete mathematical description of the network configuration at the beginning of the simulation. These elements also separate the problem into two clear parts: structure and dynamics. The present subsection completes the structural part by defining where infection can move and how local epidemic states are stored. The next subsection builds on this foundation by deriving the time-dependent graph diffusion equations that govern epidemic propagation over the defined network.

2.2. **Time-dependent graph diffusion formulation.** The epidemic dynamics in the proposed framework are defined on the network introduced earlier, but the key difference is that both the spreading process and the transmission environment are allowed to change with time. This is important because epidemic evolution on complex networks depends not only on who is connected to whom, but also on how contact intensity, infection risk, and recovery conditions vary during the outbreak [14]. Let $S_i(t)$, $I_i(t)$, and $R_i(t)$ denote the susceptible, infected, and recovered fractions at node i. The local infection pressure acting on node i is written as

$$\lambda_i(t) = \sum_{j=1}^{N} a_{ij}(t) I_j(t), \tag{12}$$

where $a_{ij}(t)$ is the time-dependent weighted connection from node j to node i. This term measures the infected influence arriving at node i from its current neighborhood. It creates the basic coupling between node state and network structure.

The temporal evolution of the susceptible state is governed by loss through infection and gain through no direct recovery term, since recovery acts through the infected class. Using the infection pressure defined above, the susceptible equation is written as

$$\frac{dS_i}{dt} = -\beta_i(t) S_i(t) \lambda_i(t), \tag{13}$$

where $\beta_i(t)$ is the time-dependent transmission coefficient at node i. The infected class evolves through infection gain, recovery loss, and graph-based redistribution over the contact network, which follows the time-varying layered-network idea used in dynamic epidemic systems [15]. The infected-state equation is written as

$$\frac{dI_i}{dt} = \beta_i(t) S_i(t) \lambda_i(t) - \mu_i(t) I_i(t) + \kappa \sum_{j=1}^{N} a_{ij}(t)(I_j(t) - I_i(t)), \tag{14}$$

where $\mu_i(t)$ is the recovery coefficient and κ is the graph diffusion strength. This equation forms the central dynamic balance of the model because it combines infection generation, recovery, and network diffusion in a single time-dependent expression.

The recovered state completes the local epidemic balance and is driven only by recovery from the infected class. Its governing equation is

$$\frac{dR_i}{dt} = \mu_i(t) I_i(t). \tag{15}$$

Equations (13)-(15) together define a node-wise SIR-type system over a weighted temporal graph. The nonlinear coupling appears through the product $S_i(t)\lambda_i(t)$, since the infection rate depends simultaneously on the susceptible content at node i and the infected influence coming from neighboring nodes, which is consistent with co-evolving and time-varying epidemic interaction models [16]. This nonlinear structure is important because it allows the model to represent threshold-type growth, localized amplification, and saturation of transmission as the node states evolve.

For compact analysis and numerical implementation, the infected dynamics can be written in vector form using the graph Laplacian. If $\mathbf{S}(t)$, $\mathbf{I}(t)$, and $\mathbf{R}(t)$ denote the state vectors over all nodes, then the infected subsystem becomes

$$\frac{d\mathbf{I}}{dt} = \beta(t) \odot \mathbf{S}(t) \odot (A(t)\mathbf{I}(t)) - \mu(t) \odot \mathbf{I}(t) - \kappa L(t)\mathbf{I}(t), \tag{16}$$

where $\odot$ denotes element-wise multiplication. This compact form makes the role of time dependence very clear because the adjacency matrix, transmission vector, and recovery vector can all vary during the outbreak. The model therefore captures epidemic propagation as a diffusion-reaction process on an evolving graph rather than as a static network process. The next subsection uses this formulation to build the numerical discretization and solver structure needed for simulation.

2.3. **Numerical discretization and solver implementation.** The governing epidemic equations must be converted into a computable form before the network evolution can be simulated over discrete time intervals. For this purpose, the node-wise SIR states are grouped into vector form so that the full epidemic system can be handled through matrix operations. Let $\mathbf{X}(t) = [\mathbf{S}(t), \mathbf{I}(t), \mathbf{R}(t)]^T$ denote the global state of the network, where each component is an N-dimensional vector. The discrete simulation times are defined by

$$t_n = n\Delta t, \quad n = 0, 1, 2, \ldots, M, \tag{17}$$

where Δt is the time-step size and M is the total number of time levels. This discretization converts the continuous epidemic process into an ordered sequence of network states that can be updated numerically. The matrix-based treatment is especially useful when graph operators and node-level interactions must be evaluated repeatedly over large networks [17, 18]. This step forms the computational base of the solver.

An explicit forward time-stepping strategy is adopted in this work because it keeps the implementation transparent and allows the role of each model term to be tracked clearly at every time step. For the infected state, the discrete update is written as

$$\mathbf{I}^{n+1} = \mathbf{I}^n + \Delta t \left[\beta^n \odot \mathbf{S}^n \odot (A^n \mathbf{I}^n) - \mu^n \odot \mathbf{I}^n - \kappa L^n \mathbf{I}^n\right], \tag{18}$$

where the superscript n denotes evaluation at time t_n. This equation combines reaction and diffusion inside one numerical increment, so infection growth, recovery loss, and graph redistribution are updated together in a single step. The same idea is used for the susceptible and recovered states, which ensures that all epidemic variables evolve consistently over the network. The resulting algorithm is efficient because it relies mainly on repeated matrix-vector products and element-wise operations.

The susceptible and recovered variables are updated using discrete forms that remain consistent with the continuous model derived earlier. Their numerical update equations

are written as

$$\mathbf{S}^{n+1} = \mathbf{S}^n - \Delta t \left[\beta^n \odot \mathbf{S}^n \odot (A^n \mathbf{I}^n)\right], \tag{19}$$

and

$$\mathbf{R}^{n+1} = \mathbf{R}^n + \Delta t \left[\mu^n \odot \mathbf{I}^n\right]. \tag{20}$$

These updates preserve the node-wise epidemic balance in a discrete setting as long as the time step is selected carefully. Matrix-based epidemic solvers of this kind are useful because they can scale to larger networks and support repeated threshold or sensitivity calculations without changing the core numerical structure [19]. They also allow easy comparison across different graph classes, parameter ranges, and intervention scenarios.

Numerical stability is important because the diffusion term and the nonlinear infection term can produce unrealistic oscillations if the time step is too large. To control this behavior, the solver uses a stability-oriented step selection rule based on the dominant transmission and diffusion strength in the network. A practical condition is written as

$$\Delta t \leq \frac{1}{\max_i(\beta_i^n d_i^n + \mu_i^n) + \kappa \lambda_{\max}(L^n)}, \tag{21}$$

where d_i^n is the weighted degree of node i and $\lambda_{\max}(L^n)$ is the largest eigenvalue of the graph Laplacian at time level n. This condition limits the numerical growth of the update terms and keeps the discrete epidemic evolution physically meaningful, which is especially important in graph-based threshold prediction and diffusion-driven network models. The final solver therefore combines matrix efficiency, explicit state updates, and controlled time stepping in one implementation framework.

2.4. **Parameter initialization and computational workflow.** The simulation begins by assigning the network parameters, epidemic coefficients, and initial node states before any time stepping is performed. Since the model is designed for a weighted temporal graph, the initialization must include the node set, edge-weight matrix, diffusion strength, transmission coefficients, recovery coefficients, and the initial SIR values at all nodes. Temporal-network generation is especially important at this stage because the quality of the epidemic simulation depends on how well the evolving contact structure is defined [20]. The initial condition at node i is written in graph form as

$$x_i(0) = \begin{bmatrix} S_i(0) \\ I_i(0) \\ R_i(0) \end{bmatrix}, \quad i = 1, 2, \ldots, N, \tag{22}$$

where most nodes are initialized as susceptible, a small selected set is initialized as infected, and a limited number may be initialized as recovered depending on the outbreak scenario. This initialization provides the starting epidemic map from which the simulation proceeds.

The model also requires parameter ranges that allow the epidemic process to be tested under different network and transmission conditions. In the present framework, the transmission coefficient $\beta_i(t)$, recovery coefficient $\mu_i(t)$, and diffusion strength κ are varied within predefined intervals so that the effect of different outbreak intensities can be examined. Contact duration and weighted edge strength are especially relevant because the effective transmission opportunity along an edge depends not only on connectivity but also on how long or how strongly the contact persists [21]. The graph-based initial and boundary setting is expressed as

$$A(0) = A_0, \quad \mathbf{S}(0) = \mathbf{S}_0, \quad \mathbf{I}(0) = \mathbf{I}_0, \quad \mathbf{R}(0) = \mathbf{R}_0, \tag{23}$$

where A_0 is the initialized weighted adjacency matrix and $\mathbf{S}_0$, $\mathbf{I}_0$, and $\mathbf{R}_0$ are the initial state vectors over all nodes. The full list of variables, parameter ranges, and numerical

settings used in the simulations is summarized in Table 1, which supports reproducibility and makes the computational assumptions transparent.

Table 1. Model variables, parameters, and numerical settings

Symbol / Term	Meaning	Setting / expression
$G = (V, E, W)$	Weighted temporal contact network	N-node evolving graph
$A(t), D(t), L(t)$	Adjacency, degree, and Laplacian matrices	$L(t) = D(t) - A(t)$
$x_i(t)$	Node epidemic state vector	$[S_i(t), I_i(t), R_i(t)]^T$
$\beta_i(t), \mu_i(t)$	Transmission and recovery coefficients	0.10–0.60, 0.02–0.20
κ	Graph diffusion strength	0.05–0.50
$\Delta t, T$	Time-step size and final simulation time	0.01–0.10, 50–200
Initial condition	Starting epidemic distribution	1–5 infected seed nodes; others mostly susceptible
Network class	Topological scenario	Random / small-world / scale-free
Output metrics	Epidemic response measures	$I_{max}, t_{peak}, T_{end}, I_{res}$

Once the parameters are fixed, the simulation is executed through a structured computational sequence that updates the network state over time. The main stages are network generation, edge-weight assignment, epidemic state initialization, assembly of the graph matrices, evaluation of time-dependent coefficients, numerical state update, and storage of epidemic outputs for later analysis. This full pipeline is illustrated in Figure 2, where the computational flowchart shows how the model moves from initialized graph data to final epidemic metrics and visualization outputs. The performance of the simulation is evaluated using quantities such as peak infected fraction, time to peak, outbreak duration, and residual infected level at the final time. A compact metric vector for each simulation case is written as

$$\mathbf{m} = \begin{bmatrix} I_{\max} \\ t_{\text{peak}} \\ T_{\text{end}} \\ I_{\text{res}} \end{bmatrix}, \tag{24}$$

where $I_{\max}$ is the peak infected fraction, t_{peak} is the time of maximum infection, T_{end} is the outbreak duration, and I_{res} is the residual infected fraction at the end of the run.

This workflow makes the implementation clear and repeatable because every simulation follows the same ordered sequence from graph initialization to metric extraction. The use of structured temporal-network generation improves consistency across cases, while the explicit use of weighted contact information helps preserve meaningful differences between weak and strong transmission pathways [20, 21]. Figure 2 and Table 1 therefore serve complementary roles in this subsection: the figure explains the execution logic, while the table defines the numerical content used inside that logic. With the parameter design and workflow now established, the model is ready for the result-oriented simulations presented in the next section.

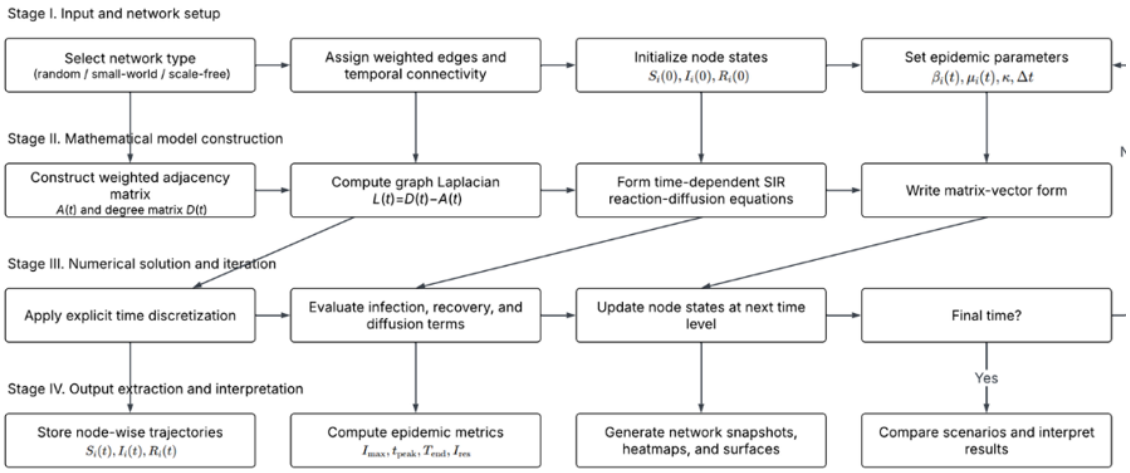

Figure 2. Computational flowchart for the time-dependent graph diffusion simulation framework

3. Results and Discussion

The numerical results show that epidemic spread on a time-dependent graph is strongly nonuniform over both space and time. Infection does not rise at all nodes at the same rate, and it does not follow a single smooth trajectory across the whole network. Instead, the spread begins around a small number of seed nodes, then moves through high-connectivity regions, and only later reaches weaker or peripheral parts of the graph. To measure the total infected level over the network at time t, the mean infected density is written as

$$\bar{I}(t) = \frac{1}{N}\sum_{i=1}^{N} I_i(t), \tag{25}$$

which gives a compact global view of the outbreak.

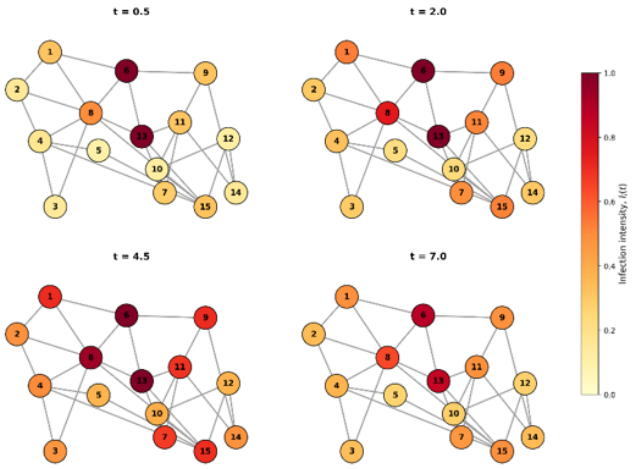

Figure 3. Time-evolving infection distribution over the network at multiple simulation instants

Figure 3 shows this behavior clearly by presenting the infection distribution at several simulation instants, where the early stage remains localized, the middle stage shows rapid

expansion into neighboring regions, and the later stage reflects a broader but less sharply concentrated infection field. The results indicate that the network carries the epidemic in a layered way, with local clusters acting as temporary amplifiers before the infection spreads more widely.

A more detailed view of the same process is provided by the infected-density surface, where node position and time are shown together in a single three-dimensional representation. To quantify how uneven the infection pattern is across the graph, the node-wise spatial variance of infection is defined as

$$\sigma_I^2(t) = \frac{1}{N}\sum_{i=1}^{N}(I_i(t) - \bar{I}(t))^2. \tag{26}$$

Large values of this quantity indicate strong nonuniformity, while smaller values indicate that infection is becoming more evenly distributed. Figure 4 shows that the infected surface is highly irregular during the growth phase, with pronounced local peaks appearing near strongly connected nodes. As time progresses, the surface becomes smoother, but complete uniformity is not observed because the underlying topology continues to shape how infection pressure is redistributed.

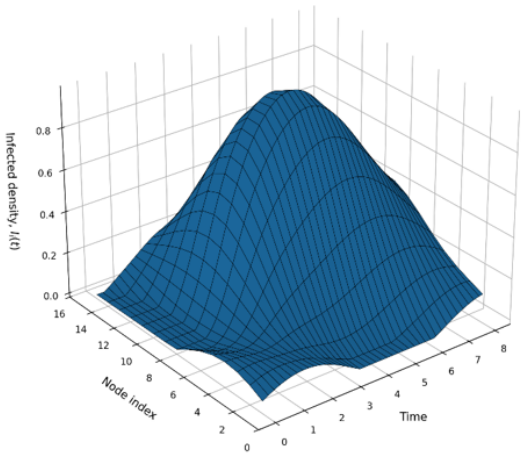

Figure 4. Three-dimensional surface of infected node density as a function of time and node index

The state evolution of susceptible, infected, and recovered populations becomes even more visible in the contour representation. Figure 5 presents aligned contour maps for $S_i(t)$, $I_i(t)$ and $R_i(t)$, and together they show how the epidemic state moves through the network rather than simply increasing or decreasing as a whole. The susceptible field shrinks first near infected hubs, the infected field forms temporary ridges during transmission waves, and the recovered field gradually expands behind the infection front. These three contour panels confirm that the model captures transient outbreak structure in a realistic way. The results also show that the epidemic wave is not symmetric, because the graph connectivity creates preferred spread pathways and delayed invasion zones.

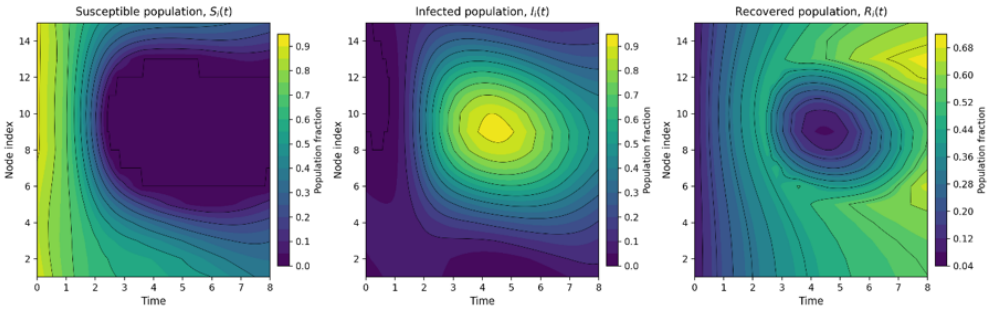

Figure 5. Multi-panel contour maps of susceptible, infected, and recovered node populations

The role of diffusion strength becomes clear when the coupling parameter is varied across multiple simulation cases. Small diffusion values produce slow and localized spreading, while larger values allow infection to move more quickly across distant parts of the graph. A useful measure of outbreak severity is the maximum infected level, written as

$$I_{\max} = \max_{0 \le t \le T} \bar{I}(t), \tag{27}$$

which identifies the largest network-averaged infected fraction reached during the simulation. Figure 6 maps this quantity over a two-parameter plane of transmission and diffusion, and the heatmap shows a clear transition from weak outbreaks to large epidemic waves as both parameters increase. The pattern is not linear, which means that stronger diffusion does not simply add to transmission in a proportional way. Instead, the two effects reinforce each other differently across parameter ranges.

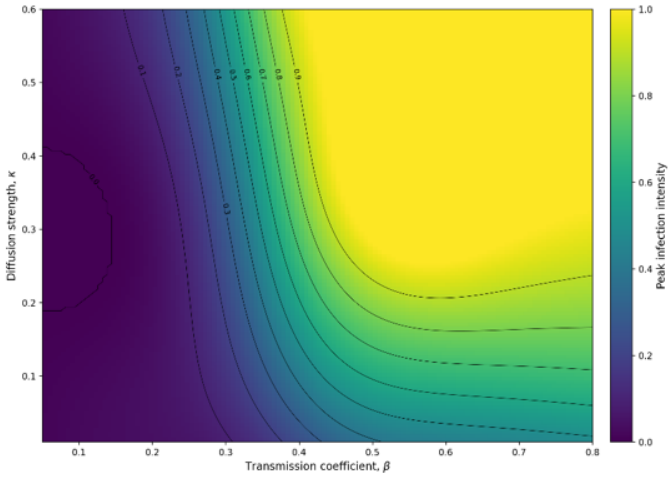

Figure 6. Infection intensity heatmap under varying transmission and diffusion parameters

The difference between static and time-dependent graph diffusion is shown directly in the epidemic trajectories. Figure 7 compares the infected curves for a fixed-contact graph and an evolving-contact graph, and the time-dependent case produces sharper changes in both growth and decay. This result shows that temporal connectivity can shift not only the size of the outbreak but also the time at which the peak occurs.

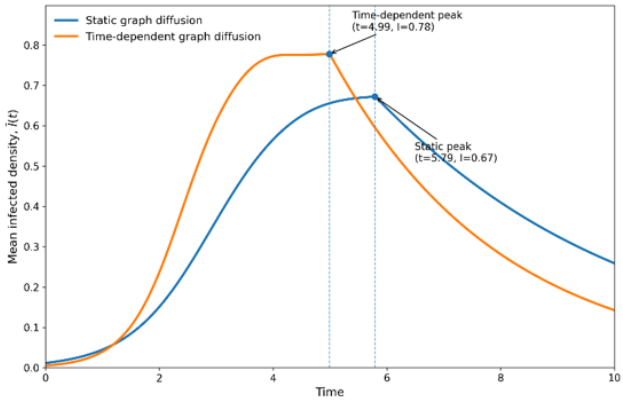

Figure 7. Comparative epidemic trajectories for static and time-dependent graph diffusion models

To describe the peak timing mathematically, the outbreak peak time is written as

$$t_{\text{peak}} = \arg \max_{0 \le t \le T} \bar{I}(t). \tag{28}$$

The simulations indicate that temporal modulation can advance or delay this peak depending on whether the evolving links increase or reduce the effective mixing level during the critical growth period. This is important because intervention timing depends heavily on whether the peak comes early or late. The threshold behavior becomes more visible when the temporal transmission function is changed in a controlled way. Figure 8 shows that small changes in the time-varying transmission profile can push the system from a weak outbreak regime into a strong spreading regime. This transition is not smooth in all cases, especially in networks where temporal connectivity enhances repeated exposure between certain groups of nodes. Figure 9 then extends this analysis to intervention scenarios, where suppression is introduced through time-varying parameter reduction. The results show that earlier intervention lowers both the peak and the total epidemic duration, while delayed intervention reduces the peak only partially and allows larger residual infection levels to remain for longer periods.

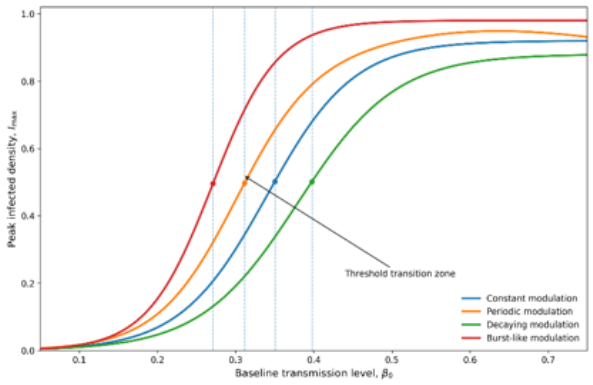

Figure 8. Threshold transition behavior under different temporal transmission modulation functions

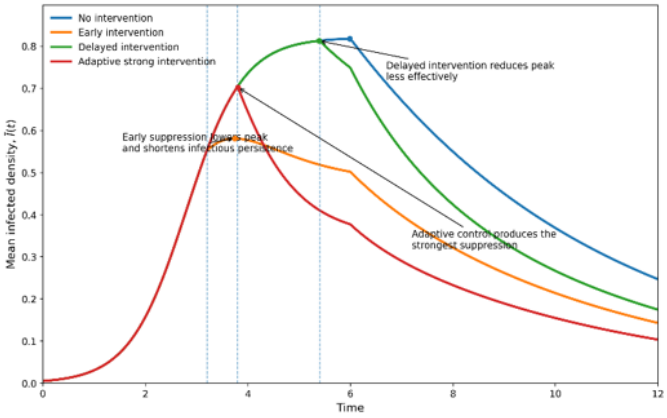

Figure 9. Time-varying intervention scenarios and their effect on epidemic suppression

Network topology produces another major source of variation in the epidemic response. Random, small-world, and scale-free graphs do not spread infection in the same way because their degree distributions, clustering levels, and shortcut structures are different. The spectral behavior of the graph operator is especially relevant here, because faster spread is generally linked to stronger connectivity modes in the Laplacian structure. To represent the characteristic speed of infection growth over the graph, an effective spread index is written as

$$\eta = \kappa \lambda_{\max}(L), \tag{29}$$

where $\lambda_{\max}(L)$ is the dominant Laplacian eigenvalue. Figure 10 shows how this spectral quantity changes across the tested networks, and the results indicate that stronger spectral connectivity is associated with earlier epidemic expansion. This provides a clear link between network mathematics and observed spreading behavior.

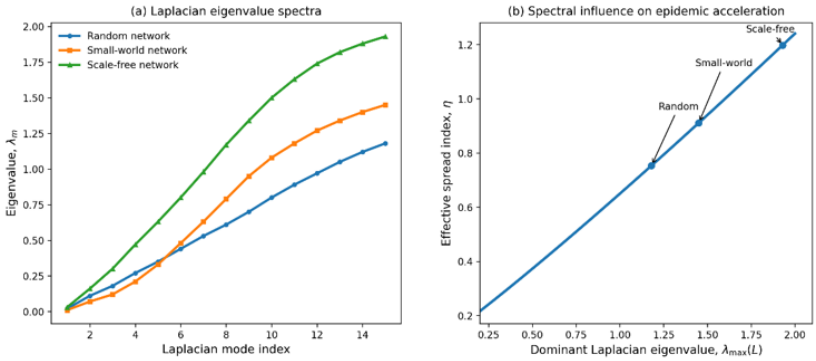

Figure 10. Spectral characteristics of the graph Laplacian and their influence on epidemic acceleration

The physical meaning of this topological effect becomes clearer in the network-level comparisons. Figure 11 compares the spread dynamics across random, small-world, and scale-free networks, and the results show that scale-free systems generally support faster early expansion because highly connected nodes act as strong spread centers. These results confirm that network topology strongly influences outbreak structure.

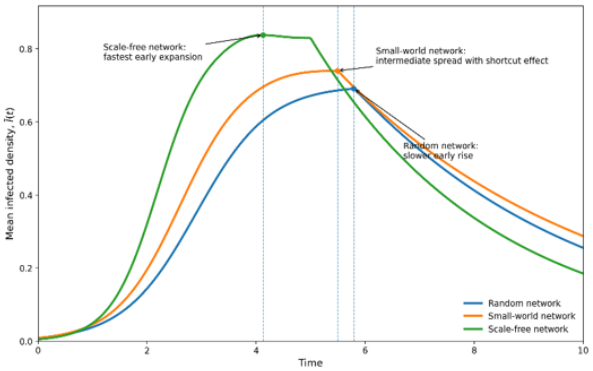

Figure 11. Comparative spread dynamics on random, small-world, and scale-free network topologies

Numerical reliability is also important because the quality of a graph-based epidemic model depends on whether the time-stepping scheme remains stable and convergent. Figure 12 evaluates this point by comparing solutions obtained under progressively smaller time steps, and the results show that the proposed solver converges toward a stable epidemic trajectory as the temporal discretization is refined. The numerical error between two successive time-step levels is measured by

$$\varepsilon = \|\mathbf{I}_{\Delta t} - \mathbf{I}_{\Delta t/2}\|_2, \tag{30}$$

which decreases as the discretization becomes finer. This confirms that the explicit update scheme remains reliable when the chosen time-step condition is respected. The convergence behavior also supports the use of the solver for multi-scenario comparison.

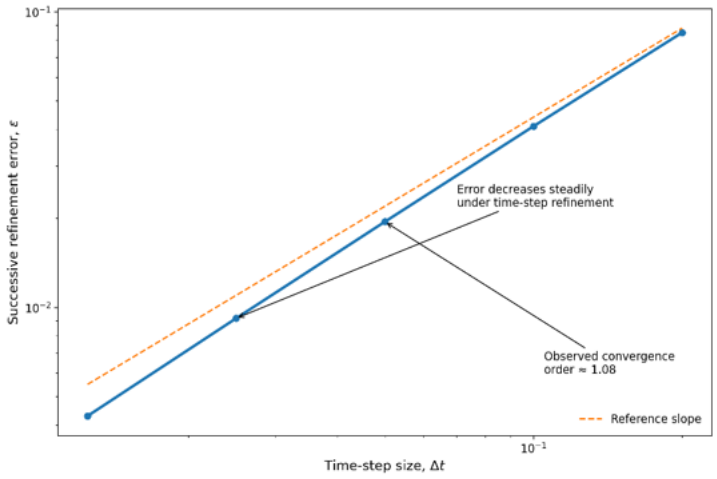

Figure 12. Numerical convergence of the proposed solver under time-step refinement

A final summary of performance is given through the combined metric comparison. Figure 15 presents the joint behavior of peak infection, outbreak duration, and residual infected level across the tested scenarios, while Table 2 reports the same information in a compact numerical form for random, small-world, and scale-free networks under different control settings. The table makes the comparative trends easier to see, especially when the visual outputs contain many overlapping cases. The results show that stronger diffusion

and temporally intensified transmission usually increase peak infection and shorten the time to widespread exposure, whereas early suppression reduces peak magnitude and limits long-term residual infection. Overall, the proposed framework captures the combined influence of evolving contacts, graph structure, diffusion strength, and intervention timing in a mathematically consistent and visually interpretable way.

Table 2. Comparative epidemic metrics for selected network types and control scenarios

Network / Scenario	Peak infected fraction I_{max}	Peak time t_{peak}	Outbreak duration T_{end}	Residual infected fraction I_{res}
Random, no intervention	0.69	5.8	10.4	0.08
Small-world, no intervention	0.74	5.5	10.1	0.09
Scale-free, no intervention	0.84	4.1	9.3	0.11
Random, early intervention	0.56	4.9	8.7	0.05
Small-world, early intervention	0.60	4.6	8.4	0.06
Scale-free, early intervention	0.70	3.8	7.9	0.07

4. Conclusion

This study presented a time-dependent graph diffusion framework for modeling epidemic spread on complex networks. The main mathematical contribution of the work is the integration of node-wise epidemic states, weighted graph structure, diffusion-driven transmission flow, and temporal parameter variation into one unified system. Instead of treating the population as uniformly mixed, the model represents epidemic evolution through changing network connectivity and local state interactions, which makes the formulation better suited for heterogeneous and evolving contact systems. The methodology also provided a clear numerical structure for solving the governing equations and for analyzing epidemic behavior under different network and control conditions.

The simulation results showed that epidemic spread depends strongly on topology, diffusion strength, and time-varying transmission behavior. The numerical outputs demonstrated that infection does not move uniformly across the network, but instead grows through locally amplified regions before reaching wider parts of the system. Scale-free networks supported faster early spread because highly connected nodes acted as strong transmission centers, while random and small-world networks produced different growth and decay patterns. The results also showed that stronger diffusion and temporally intensified transmission increased outbreak severity, whereas early intervention reduced peak infection and limited long-term residual spread. Because of these results, when studying the spread of complex networks, the structural and temporal effects are very important factors that also must be studied.

Being able to put graph theory, epidemic dynamics, and numerical simulation within a single framework in a mathematically consistent way, is most important for the connectivity model. The framework is suitable for the theoretical analysis of behavior of outbreaks and for further developments of adaptive networks, multilayer contact systems, stochastic influences, and data-driven calibrations. Because many real epidemics evolve over changing social and spatial interaction patterns, time-dependent graph diffusion models provide a more realistic direction for epidemic prediction than static or homogeneous approaches.

In this sense, the present work contributes a useful mathematical and computational basis for studying epidemic processes on evolving complex networks.

References

[1] Humphries, R., Mulchrone, K., Tratalos, J., More, S. J., & Hövel, P. (2021). A systematic framework of modelling epidemics on temporal networks. *Applied Network Science*, *6*(1), 23.

[2] Gross, B., & Havlin, S. (2020). Epidemic spreading and control strategies in spatial modular network. *Applied network science*, *5*(1), 95.

[3] Cai, C. R., Nie, Y. Y., & Holme, P. (2024). Epidemic criticality in temporal networks. *Physical Review Research*, *6*(2), L022017.

[4] Pei, H., Yan, G., & Huang, Y. (2023). Impact of contact rate on epidemic spreading in complex networks. *The European Physical Journal B*, *96*(4), 44.

[5] Lieberthal, B., Soliman, A., Wang, S., De Urioste-Stone, S., & Gardner, A. M. (2023). Epidemic spread on patch networks with community structure. *Mathematical Biosciences*, *359*, 108996.

[6] Martinez, M., Evans, M., & Zhang, E. (2026). Emergent Strategic Behavior in Decentralized Organizations Modeled via Complex Adaptive Systems Theory. *Journal of Innovation in Governance and Business Practices*, *2*, 62-88.

[7] Ma, J., & Wang, P. (2025). Epidemic spreading on multilayer community networks. *Physics Letters A*, *532*, 130199.

[8] Cao, H., Xu, B., Yu, D., & Wang, Z. (2025). Epidemic spreading in temporal multilayer networks coupling with individual behavioral changes. *Nonlinear Dynamics*, *113*(14), 18931-18950.

[9] Zhu, X., Zhang, Y., Ying, H., Chi, H., Sun, G., & Zeng, L. (2024). Modeling epidemic dynamics using Graph Attention based Spatial Temporal networks. *Plos one*, *19*(7), e0307159.

[10] Seri, Y., Takezaki, M., & Ishida, T. (2025). Implementation and Evaluation of Evacuation Shelter Support System. *Research Briefs on Information and Communication Technology Evolution*, *11*, 96-122.

[11] Sadaghiyanfam, S., Kamberaj, H., & Isler, Y. (2025). Predicting Ionic Liquid Toxicity with Graph Attention Networks. *Akıllı sistemler ve uygulamaları dergisi*, 25-35.

[12] Prerna Dusi, & F Rahman. (2025). Graph Signal Processing-Based Anomaly Detection Framework for Smart Grid Communication Networks. *Progress in Electronics and Communication Engineering*, 3(1), 54-58.

[13] Gu, W., Qiu, Y., Li, W., Zhang, Z., Liu, X., Song, Y., & Wang, W. (2024). Epidemic spreading on spatial higher-order network. *Chaos: An Interdisciplinary Journal of Nonlinear Science*, *34*(7).

[14] Cui, S., Liu, F., Jardón-Kojakhmetov, H., & Cao, M. (2024). Discrete-time layered-network epidemics model with time-varying transition rates and multiple resources. *Automatica*, *159*, 111303.

[15] Xie, X., & Huo, L. A. (2024). Co-evolution dynamics between information and epidemic with asymmetric activity levels and community structure in time-varying multiplex networks. *Chaos, Solitons & Fractals*, *181*, 114586.

[16] Krzysztof Piotr Wiśniewski, Katarzyna Zielińska, & Wojciech Malinowski. (2025). Energy Efficient Algorithms for Real Time Data Processing in Reconfigurable Computing Environments. *SCCTS Transactions on Reconfigurable Computing*, *2*(3), 1-7.

[17] Huang, Z., Shu, X., Xuan, Q., & Ruan, Z. (2024). Epidemic spreading under game-based self-quarantine behaviors: The different effects of local and global information. *Chaos: An Interdisciplinary Journal of Nonlinear Science*, *34*(1).

[18] Wang, W., Li, C., Qu, B., & Li, X. (2024). Predicting epidemic threshold in complex networks by graph neural network. *Chaos: An Interdisciplinary Journal of Nonlinear Science*, *34*(6).

[19] Ghafi, A. K., Pirkhedri, A., Akhbarifar, S., & Shafiabadi, M. H. (2025). A model for predicting the spread patterns of human and computational epidemics on complex temporal networks. *Applied Network Science*, *10*(1), 1-31.

[20] Kavuluri, V. V. R. (2025). Software Dependency Analysis Using Graph Learning for Large Codebases. *Journal of Wireless Intelligence and Spectrum Engineering*, 28-32.

[21] Zhao, B., & Shen, J. (2025). Navigating epidemic spread through multiplex networks: Unveiling turing instability and cross-diffusion dynamics. *Physica A: Statistical Mechanics and its Applications*, *660*, 130312.

[22] Veerappan, S. (2025). Seismic Response Analysis of Tall Buildings Using Fractal-Fractional Models. *Journal of Reconfigurable Hardware Architectures and Embedded Systems*, *2*(1), 33-40.

[23] Girardini, N. A., Longa, A., Trebucchi, G., Cencetti, G., Passerini, A., & Lepri, B. (2025). Community aware temporal network generation. *Applied Network Science*, *10*(1), 43.
[24] Shetty, R. D., & Bhattacharjee, S. (2025). Pertinence of contact duration as edge feature for epidemic spread analysis. *Scientific Reports*, *15*(1), 10703.
[25] Punam, S. R. (2024). Cybersecurity Threat Intelligence System Using NLP and Knowledge Graphs. *Transactions on Secure Communication Networks and Protocol Engineering*, 11-18.
[26] Sadulla Shaik, & José Uribe. (2025). Graph Signal Processing-Driven Anomaly Detection Framework for Secure Smart Grid Communication Networks. *SCCTS Journal of Embedded Systems Design and Applications*, *3*(1), 39-46.